

Kinetics of Palladium(0)-Allyl Interactions in the Tsuji-Trost Reaction, derived from Single-Molecule Fluorescence Microscopy

Johannes A. Menges,^[a] Alexander Grandjean,^[a] Anne Clasen,^[a] and Gregor Jung^{*[a]}

In memoriam Prof. Marcus Motzkus, Heidelberg University.

Single-molecule (SM) chemistry is devoted to unravel reaction steps which are hidden in cuvette experiments. Controversies about the substrate activation during the Tsuji-Trost deallylation motivated us to study, on the single-molecule level, the kinetics of the catalyst precursor Pd(PPh₃)₄ with our recently designed two-color fluorescent probes. Photochemical, metal-free bypass reactions were found and taken into account by the combina-

tion of spectrally separated single-molecule TIRF-microscopy and state-of-the art analysis procedures. Unselective π -complex formation ($K_D \approx 10^3 \text{ M}^{-1}$) precedes the insertion of the active catalyst into the C–OR bond (RO[−] = leaving group), indicated by the lacking immediate change of fluorescence color. The formed intermediate then decomposes on a time scale of $\geq 2 - 3 \text{ s}$ to the deallylated product.

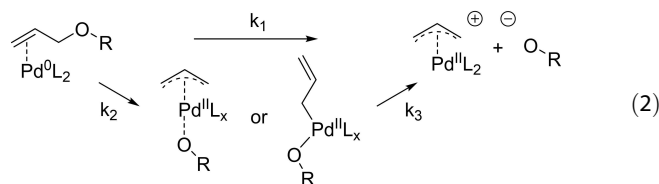
Introduction

Over the last decade, single-molecule fluorescence spectroscopy (SMFS) emerged as a tool to bring insights into the microscopic behavior of molecular, chemical systems.^[1–5] When ensemble measurements conceal uncommon events, single-molecule observation has the potential to provide a deeper understanding of chemical processes.^[6–8] In these first studies, it was shown that even text book reactions can show furcations of reaction pathways, still leading to an identical product.^[9] Hidden intermediates^[10] or static disorder is revealed for single nanoparticles and enzymes.^[11,12] Reactivity mapping of heterogeneous catalysts has been accomplished with spatial resolution.^[13] Ligand exchange^[14,15] and polymerization^[16] reactions have been investigated in model systems for homogeneous catalysis.^[17] To further advance this field in direction of recent synthetic chemistry, we previously introduced multi-emissive probes for the so-called participant approach.^[18–21] The Tsuji-Trost allylic substitution provides an example of a well-known and widely-used organometallic reaction.^[22–24] We have chosen to study this reaction as only few components are involved and there are still some mechanistic details under discussion. The putative active catalyst is PdL₂ (L = Ligand, e.g. PPh₃), which is formed during dissociation from a Pd⁰-

precursor like Pd(PPh₃)₄.^[25] The catalytic cycle then consists of two separable reactions, the displacement of allylic substrates,^[26] also utilized for cleavage of allyl protective groups,^[27] and the allylic alkylation.^[28,29] This second half of the catalytic cycle is described by the nucleophilic attack of a wide variety of nucleophiles^[22] on the Pd-allyl-complex, finally forming C–C, C–N and C–O bonds.^[30] In our study, we focus on the primary activation step. Here, the catalytic active Pd⁰L₂ species stands in equilibrium with a Pd- η^2 -allyl-complex in equation (1).



Via this transient complex, a cationic η^3 -allyl-complex is yielded. Especially for this part of the reaction, the Pd-mediated deallylation, ambiguity exists regarding the progression of the oxidative addition of allylic substrates to Pd⁰. The latter step may proceed similar to a S_N2 reaction^[31] with immediate release of the leaving group [eq. (2)].



Alternatively, the Pd-center may insert into the C–OR-bond^[30,32] (RO[−] = leaving group). Here, an oxidative association with formation of either a π -allylic η^3 -intermediate or a η^1 -Pd-complex^[33,34] are proposed, with the leaving group temporarily bound in the ligand sphere. From these intermediates a consecutive dissociation step then is expected.^[35] With the aim of obtaining new insights into the mechanisms of leaving group release, we studied the

[a] J. A. Menges, A. Grandjean, A. Clasen, Prof. G. Jung
Department of Biophysical Chemistry
Saarland University
Building B2 2
66123 Saarbrücken (Germany)
E-mail: g.jung@mx.uni-saarland.de

Supporting information for this article is available on the WWW under <https://doi.org/10.1002/cctc.202000032>

© 2020 The Authors. Published by Wiley-VCH Verlag GmbH & Co. KGaA.
This is an open access article under the terms of the Creative Commons Attribution License, which permits use, distribution and reproduction in any medium, provided the original work is properly cited.

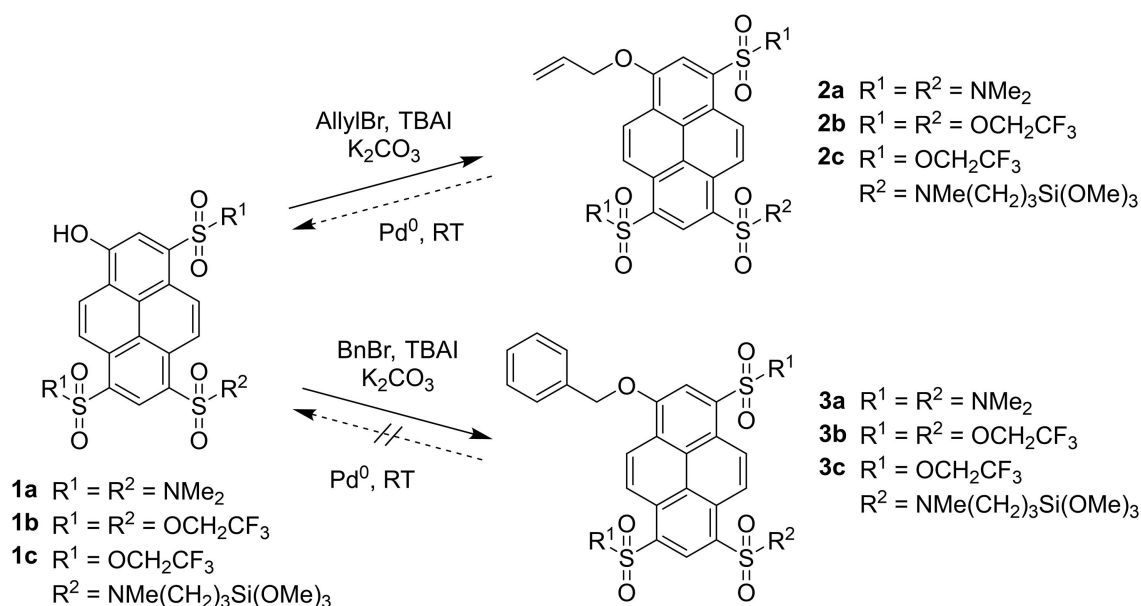
interactions of Pd⁰ with our recently introduced, dual-emissive and immobilizable substrates:^[36] During this reaction, tetrakis(triphenylphosphine)-palladium(0) (Pd⁰) causes a strong bathochromic shift in substrate fluorescence (SI Figure S2).

To probe the early events during the interaction of Pd⁰ with the substrate, i.e. the equilibrium of complex formation, we used time-correlated single photon counting (TCSPC)^[37] and analyzed the quenching behavior by a Stern-Volmer (SV)-analysis. Monitoring fluorescence emission of individual reactive chromophores with two-channel detection in total-internal reflection fluorescence microscopy (TIRFM)^[38] should then enable conclusions about the role of Pd during chemical transformation. In addition, we investigated several data analysis routines for adaption to irreversible reactions. Hidden Markov modelling^[39] or Bayesian statistical analysis,^[40] very well suited for the analysis of Förster resonance energy transfer (FRET) trajectories in equilibria, allow for extracting kinetic or mechanistic data from two channel SM fluorescence trajectories. Problems may occur when applied to a single reaction step with superimposed fluorescence quenching. We therefore searched for an unbiased statistical analysis of obtained single-molecule data. At first, we pursued noise-cancelling auto- and cross-correlation analyses of single particle emission^[41] for extraction of substrate decay and product rise. Subsequently, we compared the outcome with the results from analyzing the histograms of substrate fluorescence termination and product fluorescence formation events. With these methods, kinetic information of the reaction steps in equation (1) and (2) could be extracted, but photochemical bypass reactions were deciphered as well.

Results and Discussion

We synthesized pyrene-based, reactive fluorophores **2a**, **2b** and **2c** from **1a**, **1b** and **1c** according to existing procedures^[36,37] (scheme 1). The benzylated probes **3a**, **3b** and **3c** were synthesized in a similar fashion (SI pp.: 4–7). Compounds **2a,b** and **3a,b** were used for kinetic experiments in cuvette whereas **2c** and **3c** were used for immobilization on quartz surfaces prior to SM visualization.^[36] All probes **2a**, **2b**, **3a** and **3b** were stable in ethanol at standard conditions in the time span of these experiments. In steady-state experiments with **3a** and **3b**, no product formation at RT was noticed, neither in presence of Pd⁰, nor in combination with Pd⁰ and the nucleophiles ethylmalonate and acetoacetate^[28] (SI Figure S3). Due to the lacking reactivity at RT towards Pd⁰, the benzylated derivatives served as control probes in this study. Electronic spectra and photophysical properties of all compounds were determined and are compiled in table S1 (SI Figure S1).

We performed steady-state and time resolved measurements in solution for characterizing the Pd⁰ interaction with the substrate prior to the reaction. With addition of various amounts of Pd⁰ up to a saturated solution (150 μM), fluorescence emission of unreactive **3a**, **3b** and **1b** was quenched (SI Figure S4). Association constants K_{SV} of $\sim 10^3 M^{-1}$ were obtained from a SV plot^[42] (Figure 1a). Fluorescence lifetimes of **2a**, **2b** and **3a**, **3b**, on the other hand, remained unchanged shortly after addition of Pd⁰ (SI Figure S5). These findings indicate static quenching by Pd⁰, i.e. complex formation.^[43]



Scheme 1. Synthesis of reactive (**2a,b,c**) and reference probes (**3a,b,c**) for the Tsuji-Trost deallylation reaction^[36,37] performed in acetone or dimethylformamide.

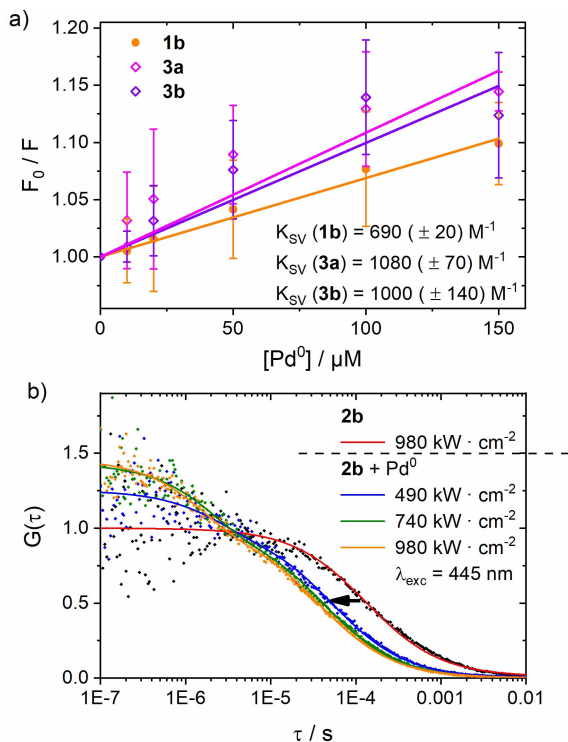


Figure 1. a) Stern-Volmer plots of the fluorescence quenching of **3a**, **3b** and **1b** by Pd^0 ; b) Fluorescence correlation functions of **2b**, the arrow depicts the change from pure ethanol to measurements with Pd^0 , dependent on varying illumination intensities (extracted from SI Figure S7), solid lines represent fits with equation (3).

Fluorescence Correlation Spectroscopy (FCS)

FCS was performed in oxygen-free ethanol to further determine the underlying kinetics (SI pp.17). We used compounds **3b** and **1b** as control probes, with enough brightness and photostability for FCS under short wavelength excitation ($\lambda_{\text{exc}}=445$ nm and 488 nm; SI Figure S7). Moreover, reactive **2b** was investigated as well, shortly after addition of Pd^0 . As the measurement time was limited due to the consumption of **2b**, we exploited high excitation intensities for obtaining reasonable FCS curves (Figure 1b). Autocorrelation curves revealed a dark state in the presence of Pd^0 , the ligand PPh_3 (1 mM) and only in the absence of oxygen. Consequently, strong fluorescence fluctuations cannot unambiguously be traced back to the interaction with the catalyst.

Moreover, since the amplitude and the contrast of the fast fluctuations depend on illumination intensities, these observations point to typical light driven processes.^[44] However, photochemical release of a phosphine ligand^[45] could not be excluded. Equation (3) therefore represents the kinetic description of a reversible dark state formation from autocorrelation curves.

$$G(\tau) = \frac{1}{\langle N \rangle} \cdot \left(\frac{1}{1 + \frac{\tau}{\tau_{\text{diff}}}} \right) \cdot \left(1 + \frac{k_{\text{dark, eff}}}{k_{\text{bright}}} \cdot e^{-(k_{\text{dark, eff}} + k_{\text{bright}}) \cdot \tau} \right) \quad (3)$$

Through application of equation (3), effective dark state formation and decomposition rates $k_{\text{dark, eff}}$ and k_{bright} in the μs -time regime were obtained. While on the μs -time scale hardly any significant differences between **3b** and **2b** are found in FCS, we noticed a distinct reduction of apparent diffusion time τ_{diff} from $160 (\pm 36) \mu\text{s}$ to $< 40 (\pm 4) \mu\text{s}$ upon addition of Pd^0 only in **2b**. Although the interpretation of apparent τ_{diff} requires caution,^[46] we conclude that the extracted $k \approx 1.5 \cdot 10^4 \text{ s}^{-1}$, that is k_1 or k_2 in equation (2), appears as the upper limit for the reaction of **2b** with Pd^0L_x . Still, this upper limit is several orders of magnitude above the rate constants of the conversion in cuvette experiments ($k \approx 2 \cdot 10^{-2} \text{ s}^{-1}$),^[36] and thus may not reflect the putative $\text{S}_{\text{N}}2$ -like short cut in equation (2). In summary, the only specific interaction with Pd^0 , which is not seen in the control experiment, is the reduction of τ_{diff} . Due to resulting limited observation time window, that is the diffusion time through the detection volume, FCS in solution can neither clearly distinguish between the pathways of fluorescence loss in eq. (2) nor does provide the kinetics of eq. (1) in its present configuration.

TIRF-microscopy

For exploring the Pd^0 interaction during chemical conversion, the deallylation reaction was visualized on the SM level. Simultaneous observation of substrate and product with low background was achieved with a prism-based TIR^[38] excitation in a custom built setup^[36,47] and dual-channel detection. Excitation and emission spectra of silanes **1c** and **2c** in solution as well as utilized laser lines and detection channels are shown in Figure 2a. Dyes **1c**, **2c** and **3c** were immobilized on a, with methylsilane passivated quartz surface, as described before,^[36] leading to 1_{imm} (product), 2_{imm} (reactive substrate), and 3_{imm} (reference substrate) (SI Figure S10). Movies (100 ms/frame) of immobilized substrates 2_{imm} and 3_{imm} were recorded in ethanol before, during and after addition of $100 \mu\text{M Pd}^0$. With 2_{imm} , a clear shift of emitting molecules from the “blue” (417–477 nm) to the “orange” (500–600 nm) detection channel was observed, which was initiated by $\text{Pd}^0(\text{PPh}_3)_4$ (Figure 2b). Single-molecule fluorescence trajectories with apparent noise were extracted with the selection criterion of single bleaching steps. Finally, 1741 SM-trajectories from 9 samples of 3 independent preparations of 2_{imm} from movies during addition of Pd^0 were collected (amount of all trajectories: see SI p. 24).

To attain the temporal evolution from the starting material to product without any data preselection (except

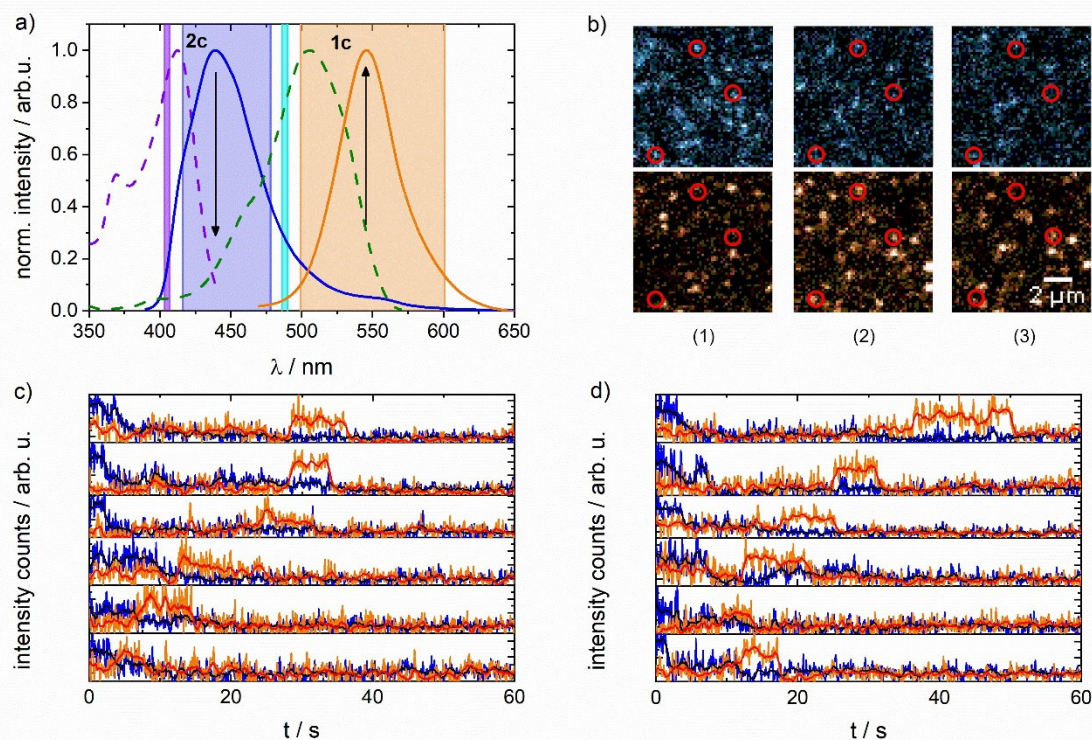


Figure 2. a) Fluorescence excitation (dashed lines) and emission (solid lines) spectra of soluted compounds **2c** (purple, blue) and **1c** (green, orange) in ethanol. Also, the utilized laser lines at 405 nm (purple) and 488 nm (cyan) are shown and spectral ranges of collected emission light from 417–477 nm (blue channel) and from 500–600 nm (orange channel); b) Images of visualized surface areas with immobilized **2_{imm}**, top: blue channel, bottom: orange channel, (1) with initiation of the reaction through Pd⁰, (2) after 5 s with Pd⁰ solution, (3) after 7 s with Pd⁰ solution, binned for 1 s (10 frames) (product molecules in first frame formed through photochemical reaction); c) Dual-Channel fluorescence trajectories of **2_{imm}** with Pd⁰ with visible color change; d) Dual-Channel fluorescence trajectories of **2_{imm}** without Pd⁰ with generation of „orange“ fluorescence (solid lines represent sliding average of fluorescence trajectories with time resolution of 1 s).

the mentioned single step in the blue channel), correlation analyses^[41] were conducted. Autocorrelation decays provide the time constant for molecule disappearance (due to reaction or photobleaching) as in FCS but also do not distinguish between these processes. Cross-correlation analysis, in contrast, is specific for the reaction and yields the time constant for product formation once a substrate molecule is identified. Moreover, artifacts and random noise are cancelled out in correlation functions^[48] and the time resolution of the acquisition frequency (10 Hz $\hat{=}$ 100 ms) is sustained in contrast to our later analyses based on binning. Emission trajectory pairs of each measurement were aligned into single paired data series. Subsequently, the overall correlation curves were calculated, which were corrected for spectral cross-talk according to the method described by Bacia et al.^[49] (SI pp. 25). The obtained corrected cross-correlation $G(\tau_{ij})$ curves of measurements with introduction of Pd⁰ show positive amplitudes (Figure 3a). In the conversion of **2_{imm}** by Pd⁰ a pronounced maximum is seen, while corresponding curves of **3_{imm}** only show a weak maximum (Figure 3a and SI Figure S11b). Kinetic constants were derived from mono- or biexponential fits of these curves, in which the rising component is interpreted as product formation. A time constant of $\tau_{form, orange}$ of 15.7 (\pm 1.5) s of

2_{imm} with presence of Pd⁰ results from this analysis (SI Figure S16). This time constant is considerably lower, by a factor 4, than the previously determined time constant of product formation in a fluorogenic approach, that is when only the formed product molecules were excited.^[36] However, if we take the competing photobleaching of the substrate **2_{imm}** into account (i.e. the decay of the blue autocorrelation functions of control **3_{imm}** and **2_{imm}** without Pd⁰, see Figure 4 and SI Figure S11), then a reduced time constant $\tau_{red} = 6.2 (\pm 1.9) s$ is expected (SI p. 34). The significant retardation from the expected 6 to the observed 16 s putatively points to an intermediate, specific to an interaction with Pd⁰, before **1_{imm}** is produced in the reaction. However, no conclusions about its nature or any reaction branching as inferred from eq. (2) can be drawn from these correlation analyses. If fluorescent intermediates with a different emission spectrum were present, then signal-pair histograms^[48,50] (SI Figure S14), created from the paired emission trajectories, could suggest their presence. However, such an analysis provided no unambiguous indication for spectrally shifted intermediates specific to the presence of Pd⁰. We therefore interpret any putative intermediate as dark state in the reaction from **2_{imm}** to **1_{imm}**. Please note that even the cross-correlation curves of **2_{imm}** without Pd⁰ shows

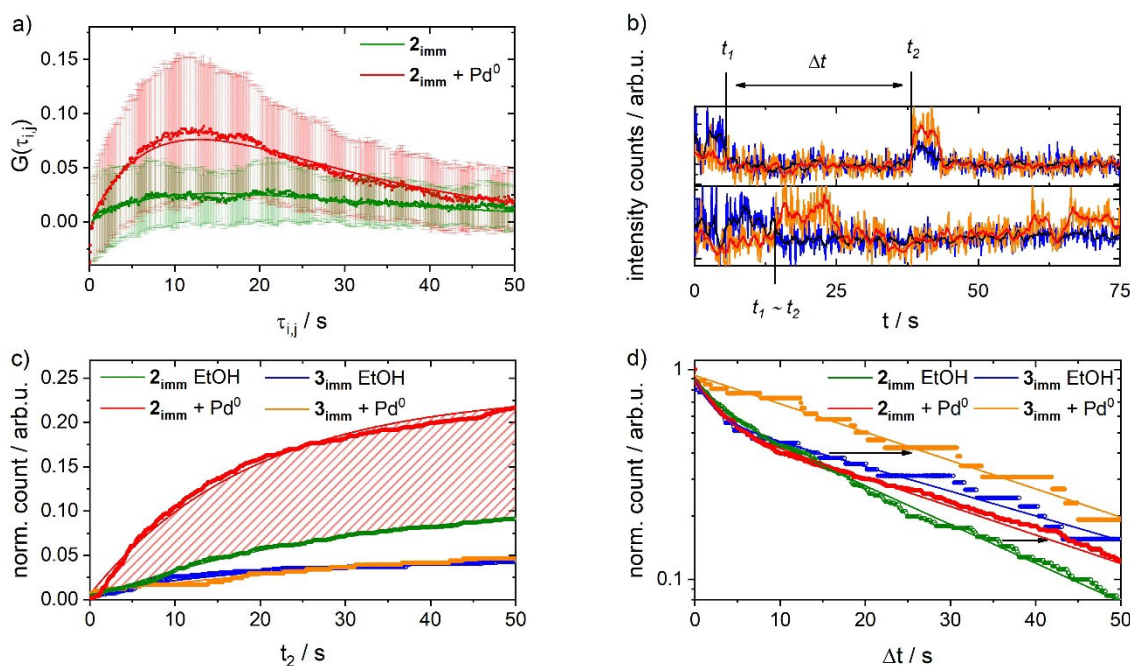


Figure 3. a) Mean cross-correlation of fluorescence intensities in the „blue“ and „orange“ channel of compound 2_{imm} without and with Pd^0 with standard deviations from 9 measurements (SI Figure S11); b) exemplary SM trajectories with sliding average over 1 s; scheme of extracted t_1 , t_2 and delay time Δt ; c) histogram of normalized product formation events t_2 regarding 2_{imm} and 3_{imm} with and without Pd^0 . The shaded area represents the additional amount of formed product 1_{imm} through influence of Pd^0 on 2_{imm} resp. the Tsuji-Trost deallylation reaction; d) histogram of lag times Δt ; arrows indicate the shift in kinetics upon addition of Pd^0 (SI Figure S16).

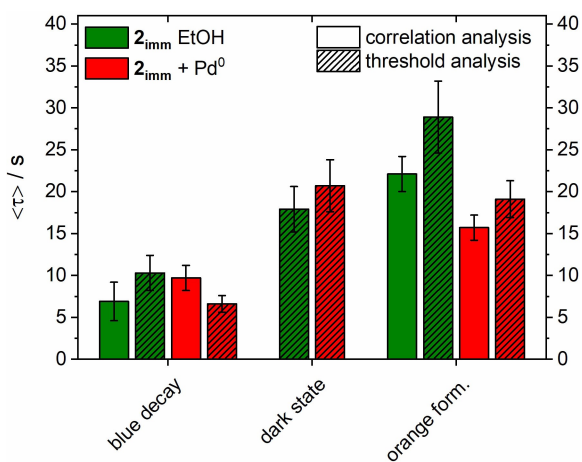


Figure 4. Obtained kinetic constants $\tau_{1/e}$ for 1. decay of blue fluorescence, 2. the lag time, i.e. dark state, 3. orange fluorescence formation from SM trajectory correlation and thresholding analyses of experiments with 2_{imm} . All data is shown in SI Figure S16.

a rising component (as does 3_{imm} with Pd^0). These latter findings are in contrast to the cuvette experiments, where only Pd^0 was able to convert **2** into **1**. A photochemical side reaction is the most likely explanation.

We subsequently chose an analysis method for extracting information out of individual trajectories, finally yielding conventional histograms. In contrast to the former analyses, any dark state is directly detected as discontinuity of fluorescence to agree with the outcome of the former

analyses. A simple algorithm was used to sort trajectories into groups of reactive and non-reactive molecules. At first, normalized intensity trajectories were transformed into a binary signal via a threshold to exclude 99% of data points, which may correspond to zero emission (SI Figure S12). Then, for recognition of product formation, the orange intensity had to exceed the corresponding threshold for at least one second (Figure 2c, d). Consecutively, all trajectories showing conversion were selected and the number of reactive molecules was determined. Roughly 28% of trajectories of 2_{imm} ($\cong 487$ of 1741 trajectories) with Pd^0 was deemed reactive with a significant rise in orange fluorescence during the observation window (Figure 2c), whereas the rest of molecules were considered to photobleach. We certainly lost a wealth of trajectories by these strict criteria and, therefore, overestimated photobleaching. In the first control experiment, that is 2_{imm} in ethanol, but without Pd^0 , however, also around 12% of fluorescence trajectories with similar behavior ($\cong 280$ of 2330 trajectories) were identified (Figure 2d). Moreover, experiments with benzylated dye 3_{imm} , also revealed approximately 6% of trajectories with rising orange fluorescence, independent of Pd^0 influence ($\cong 25$ trajectories with Pd^0 and 51 without Pd^0). These findings are in agreement with the almost vanishing cross-correlations (see Figure 3a and SI Figure S11). Interestingly, and most significant for the reaction mechanism, only a minor fraction of trajectories ($\cong 60$ of 487 reactive trajectories or 12%) exhibited a sudden color shift (~ 0.1 s).

The timepoints of substrate emission termination t_1 and product fluorescence formation t_2 were resolved from the binary fluorescence trajectories and accumulated (Figure 3b). The resulting histograms were subsequently fitted with monoexponential functions (SI p. 33 and Figure 3c, extracted from Figure S13). The kinetics of the decay of 2_{imm} , expressed by equation (4) shows a faint acceleration by Pd^0 as expected (Figure 4).

$$\langle \tau_{blue\ decay} \rangle = \frac{1}{k_{blue\ decay}} \quad (4)$$

The influence of Pd^0 on 3_{imm} is less clear, as the error margins hide any measurable effect. Altogether, the obtained rate constants are in a similar range like those of the correlation analysis (Figure 4). Conversion of $2_{imm}/3_{imm}$ to the fluorescent product support a photochemical bypass reaction for both substrates to 1_{imm} with an apparent quantum yield of about $\Phi_{ph, reac} \sim 5.5 \cdot 10^{-6}$ and $2.8 \cdot 10^{-6}$ for 2_{imm} and 3_{imm} , respectively. The most likely interpretation therefore is a photoinduced deprotection reaction, presumably via homolytic C–O cleavage^[51] or photoionization reaction^[52] (SI Scheme S2 p. 36). Its competition to the metal-organic reaction of 2_{imm} (SI p. 34) causes the seeming acceleration compared to the experiments in a fluorogenic approach.^[36]

More relevant for mechanistic insight is the analysis of the lag time Δt between the disappearance of the blue fluorescence and appearance of orange fluorescence, that is, the lifetime of the dark intermediate (Figure 3b,d). To perform an unbiased analysis of dark state evolution in regard to its mechanism, an empirical biexponential fit of Δt was utilized.

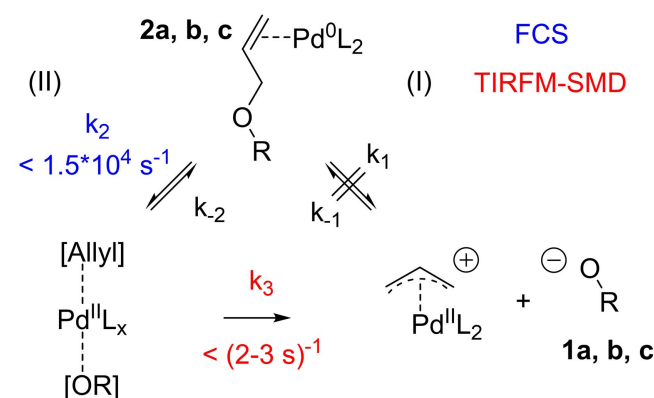
Firstly, the relative amplitudes of a fast (A_{short}) and a slow (A_{long}) decay component are resolved, normalized on the absolute number of reactive trajectories (SI Figure S16). For inert substrate 3_{imm} , addition of Pd^0 makes the short component disappear, leading to a monoexponential decay. This behavior is opposed to the reactive substrate 2_{imm} , where the amplitude of the faster decay component of the allylated 2_{imm} absolutely increases (Figure 3d). Although the relative amplitude A_{short} of the biexponential fit increases only by \sim one third (from 0.28 to 0.38), the absolute raise corresponds to 7% of all trajectories of 2_{imm} during the presence of Pd^0 (\sim 120 trajectories of 487 reactive trajectories) and, hence, to roughly half of the increase of reactive trajectories upon addition of $Pd(0)$. Thus, this faster process is related to the synthetic reaction mechanism, although it competes here with photochemical conversion. An absolute increase of the slow component is noticed as well.

Secondly, the obtained rate constants are compared. Addition of Pd^0 extends the dark state lifetime of inert substrate 3_{imm} to a single value $\tau_{dark} \approx 30 (\pm 5) s$ (Figure 3d). This time constant, however, may not necessarily reflect the binding time of Pd^0 to the substrate. Considering the benzylated derivatives **3** are not prone to conversion by Pd^0 , this latter, slower process is not related to the catalytic

cycle. This interpretation becomes important, as the same lifetime is found for the reactive substrate 2_{imm} as well. Here, Pd^0 also elongates the long component of dark state lifetime (denoted by horizontal arrow in Figure 3d). At the same time, its short component lifetime slightly shortens upon addition of Pd^0 from $\tau_{short} = 3.1 (\pm 0.5) s$ to $\tau_{short, Pd} = 2.4 (\pm 0.4) s$ opposed to its absence in the reaction of benzylated counterpart 3_{imm} (SI Figure S16b). Still, the observation of (at least) two lifetimes may also hint to more than one process being involved. The question therefore arises whether a distribution of rate constants is here a more appropriate description.

For analysis of kinetics with an intrinsic dispersion of rate constants, a Weibull analysis is employed.^[53] Here, a β -value results from a stretched exponential fit of the dataset with an effective rate constant k_{eff} . The larger the discrepancy of β from 1 is, the more pronounced is the distribution of rates around k_{eff} . Applied on the presented data, this analysis shows an increase of complexity of dark state kinetics of 2_{imm} through addition of Pd^0 , indicated by a decrease of the corresponding β -value. With the inert substrate 3_{imm} , Pd^0 exerts the opposite effect with a β -value close to one with the transition metal present (SI Figure S13d,e). One interpretation are additional contributions to reactive trajectories by e.g. the reaction of a mixture of various reactive Pd-ligand species^[25,54] or the presence of different intermediate states like η^1 or η^3 -complexes.^[33,34] In summary, no more evidence for a distinct, sudden change than before results from the kinetics dispersion.

Nevertheless, having the previously discussed lack of a fast rising component in the cross-correlation (Figure 3a) and in the t_2 - histogram (Figure 3c) as well as in direct color shifts of trajectories in mind, we therefore conclude that the vast majority of chemically relevant intermediate in the catalytic cycle has a lifetime of $2.4 (\pm 0.4) s$ or longer (scheme 2). This interpretation is further supported from the kinetics obtained from FCS experiments, which disagrees with the expected rate constants of the fluorogenic approach, and excludes a S_N2 -like shortcut from 2_{imm} to 1_{imm}



Scheme 2. Mechanism of deallylation reaction for **2a,b** and 2_{imm} with derived kinetic constants (I): allylic substitution through Pd^0 ; (II): Pd-insertion into C–O-bond.

in equation (2), rather pointing to the proposed mechanisms involving a Pd⁰ insertion into the C–O-bond.^[33,35]

Conclusion

The interaction of Pd⁰ with allyl-protected substrate molecules **2** and its chemically inert, benzylated counterpart **3** has been studied by fluorescence spectroscopy and microscopy. Steady-state unselective fluorescence quenching provides evidence for formation of a π -complex with Pd⁰L_x moieties. The reduced τ_{diff} in FCS, only observed in the allylated compounds, is suggestive of formation of a chemically relevant intermediate. SM experiments with two-channel detection were performed to cover the time regime well above 0.1 s. Noise insensitive correlation analyses and noise affected analysis of fluorescence event histograms result in similar time-constants for the substrate decay and product formation, but only the latter method shows the kinetics of presumably photoinduced dark states and reveals the existence of a Pd^{II} intermediate with a lifetime of 2–3 s. The present experiments are more in line with insertion of Pd⁰ into the C–O-bond (in a S_N2-like mechanism we would expect an instantaneous release of the product **1_{imm}**), but may reflect a selected mechanism for the Tsuji-Trost-deallylation. As our pyrene derivatives provide an excellent leaving group, the result may only be transferred to comparable substituents. Experiments with other allylated fluorophores^[55,56] are a convenient way to find out distinctions. It is yet unclear to which extent the investigated conversion, with simultaneous excitation of product and substrate agrees with the findings of our previous study based on a fluorogenic approach.^[36]

However, an intermediate, as found here with a lifetime \ll 60 s, would hardly be detected in a conventional fluorogenic approach or kinetic analyses in an ensemble and underpins the benefits of single-molecule studies.

To finally elucidate the mechanism, which takes place in synthesis, we therefore have to avoid any light-driven activation of the metal with its immediate ligand sphere, e.g. by using red labeled ligands.^[14,18,53,57] Labeled ligands, used for enantioselective chemistry, may be employed as well.^[33,34] With this development and some technical improvements, e.g. for accessing the ms-time regime,^[58] we head for resolving this widely applied metal-organic reaction on the SM-level.

Acknowledgements

This work was supported by the German Research Foundation, (DFG, project number JU650/10-1). The authors thank Reiner Wintringer (+) and Dr. Klaus Hollemeyer (Service Center Mass Spectrometry, Saarland University) for ESI-MS analysis. Also, the technical design of implemented measurement chamber and microfluidic cell by Rudolf Richter is gratefully acknowledged and Matthias Jourdain for carefully reading the manuscript.

Conflict of Interest

The authors declare no conflict of interest.

Keywords: fluorescence spectroscopy · single-molecule detection · palladium · Tsuji-Trost reaction · reaction mechanisms

- [1] M. Orrit, *Angew. Chem. Int. Ed.* **2015**, *54*, 8004–8005; *Angew. Chem.* **2015**, *127*, 8116–8117.
- [2] M. Orrit, T. Ha, V. Sandoghdar, *Chem. Soc. Rev.* **2014**, *43*, 973.
- [3] N. G. Walter, C.-Y. Huang, A. J. Manzo, M. Sobhy, *Nat. Methods* **2008**, *5*, 475–489.
- [4] T. Cordes, S. A. Blum, *Nat. Chem.* **2013**, *5*, 993.
- [5] J. C. Scaiano, A. E. Lanterna, *J. Org. Chem.* **2017**, *82*, 5011–5019.
- [6] Q. T. Easter, S. A. Blum, *Angew. Chem. Int. Ed.* **2018**, *57*, 12027–12032; *Angew. Chem.* **2018**, *130*, 12203–12208.
- [7] Y. Zhang, P. Song, Q. Fu, M. Ruan, W. Xu, *Nat. Commun.* **2014**, *5*, 1–8.
- [8] S. Dery, E. Amit, E. Gross, *Top. Catal.* **2018**, *61*, 923–939.
- [9] A. Rybina, C. Lang, M. Wirtz, K. Größmayer, A. Kurz, F. Maier, A. Schmitt, O. Trapp, G. Jung, D. P. Herten, *Angew. Chem. Int. Ed.* **2013**, *52*, 6322–6325; *Angew. Chem.* **2013**, *125*, 6445–6449.
- [10] H. Shen, X. Zhou, N. Zou, P. Chen, *J. Phys. Chem. C* **2014**, *118*, 26902–26911.
- [11] R. Ye, X. Mao, X. Sun, P. Chen, *ACS Catal.* **2019**, *9*, 1985–1992.
- [12] R. Liebherr, H. Gorris, *Molecules* **2014**, *19*, 14417–14445.
- [13] K. P. F. Janssen, G. De Cremer, R. K. Neely, A. V. Kubarev, J. Van Loon, J. A. Martens, D. E. De Vos, M. B. J. Roeflaers, J. Hofkens, *Chem. Soc. Rev.* **2014**, *43*, 990–1006.
- [14] J. D. Ng, S. P. Upadhyay, A. N. Marquard, K. M. Lupo, D. A. Hinton, N. A. Padilla, D. M. Bates, R. H. Goldsmith, *J. Am. Chem. Soc.* **2016**, *138*, 3876–3883.
- [15] A. Kiel, J. Kovacs, A. Mokhir, R. Krämer, D.-P. Herten, *Angew. Chem. Int. Ed.* **2007**, *46*, 3363–6; *Angew. Chem.* **2007**, *119*, 3427–3430.
- [16] Q. T. Easter, S. A. Blum, *Angew. Chem. Int. Ed.* **2018**, *57*, 1572–1575; *Angew. Chem.* **2018**, *130*, 1588–1591.
- [17] T. Chen, B. Dong, K. Chen, F. Zhao, X. Cheng, C. Ma, S. Lee, P. Zhang, S. H. Kang, J. W. Ha, W. Xu, N. Fang, *Chem. Rev.* **2017**, *117*, 7510–7537.
- [18] M. Wirtz, A. Grüter, F. Heib, V. Huch, J. Zapp, D.-P. Herten, M. Schmitt, G. Jung, *Methods Appl. Fluoresc.* **2015**, *3*, 44001.
- [19] M. Wirtz, A. Grüter, P. Rebmann, T. Dier, D. A. Volmer, V. Huch, G. Jung, *Chem. Commun.* **2014**, *50*, 12694–12697.
- [20] B. Finkler, I. Riemann, M. Vester, A. Grüter, F. Stracke, G. Jung, *Photochem. Photobiol. Sci.* **2016**, *15*, 1544–1557.
- [21] G. Jung, A. Schmitt, M. Jacob, B. Hinkeldey, *Ann. N. Y. Acad. Sci.* **2008**, *1130*, 131–137.
- [22] K. C. Nicolaou, P. G. Bulger, D. Sarlah, *Angew. Chem. Int. Ed.* **2005**, *44*, 4442–4489; *Angew. Chem.* **2005**, *117*, 4516–4563.
- [23] B. M. Trost, M. L. Crawley, *Chem. Rev.* **2003**, *103*, 2921–2943.
- [24] D. C. Behenna, B. M. Stoltz, *J. Am. Chem. Soc.* **2004**, *126*, 15044–15045.
- [25] M. S. G. Ahlquist, P. O. Norrby, *Angew. Chem. Int. Ed.* **2011**, *50*, 11794–11797; *Angew. Chem.* **2011**, *123*, 11998–12001.
- [26] R. O. Hutchins, K. Learn, R. P. Fulton, *Tetrahedron Lett.* **1980**, *21*, 27–30.
- [27] O. Dangles, F. Guibé, G. Balavoine, S. Lavielle, A. Marquet, *J. Org. Chem.* **1987**, *52*, 4984–4993.
- [28] T. Kajimoto, H. Takahashi, J. Tsuji, *J. Organomet. Chem.* **1970**, *23*, 275–280.
- [29] B. M. Trost, T. J. Fullerton, *J. Am. Chem. Soc.* **1973**, *95*, 292–294.
- [30] K. Tsurugi, N. Nomura, K. Aoi, *Tetrahedron Lett.* **2002**, *43*, 469–472.
- [31] B. M. Trost, D. L. Van Vranken, *Chem. Rev.* **1996**, *96*, 395–422.
- [32] D. R. Vutukuri, P. Bharathi, Z. Yu, K. Rajasekaran, M. H. Tran, S. Thayumanavan, *J. Org. Chem.* **2003**, *68*, 1146–1149.
- [33] N. H. Sherden, D. C. Behenna, S. C. Virgil, B. M. Stoltz, *Angew. Chem. Int. Ed.* **2009**, *48*, 6840–6843; *Angew. Chem.* **2009**, *121*, 6972–6975.
- [34] M. Kollmar, B. Goldfuss, M. Reggelin, F. Rominger, G. Helmchen, *Chem. Eur. J.* **2001**, *7*, 4913–4927.
- [35] A. Miyake, G. Hata, K. Takahashi, A. Miyake, *Chem. Commun.* **1970**, *2*, 1392–1393.
- [36] J. A. Menges, A. Clasen, M. Jourdain, J. Beckmann, C. Hoffmann, J. König, G. Jung, *Langmuir* **2019**, *35*, 2506–2516.

- [37] B. Finkler, C. Spies, M. Vester, F. Walte, K. Omlor, I. Riemann, M. Zimmer, F. Stracke, M. Gerhards, G. Jung, *Photochem. Photobiol. Sci.* **2014**, *13*, 548–562.
- [38] W. P. Ambrose, P. M. Goodwin, J. P. Nolan, *Cytometry* **1999**, *36*, 224–31.
- [39] I. Sgouralis, S. Pressé, *Biophys. J.* **2017**, *112*, 2021–2029.
- [40] E. Lerner, T. Cordes, A. Ingargiola, Y. Alhadid, S. Chung, X. Michalet, S. Weiss, *Science* **2018**, *359*, 1–12.
- [41] R. M. Dickson, A. B. Cubitt, R. Y. Tsien, W. E. Moerner, *Nature* **1997**, *388*, 355–358.
- [42] O. Stern, M. Volmer, *Phys. Z.* **1919**, *20*, 183–188.
- [43] J. Panchompoo, L. Aldous, M. Baker, M. I. Wallace, R. G. Compton, *Analyst* **2012**, *137*, 2054–2062.
- [44] J. Widengren, U. Mets, R. Rigler, *J. Phys. Chem.* **1995**, *99*, 13368–13379.
- [45] P. Karagiannidis, S. K. Hadjikakou, P. Aslanidis, A. Hountas, *Inorg. Chim. Acta* **1990**, *178*, 27–34.
- [46] B. Hinkeldey, A. Schmitt, G. Jung, *ChemPhysChem* **2008**, *9*, 2019–2027.
- [47] A. M. Huynh, J. Menges, M. Vester, T. Dier, V. Huch, D. A. Volmer, G. Jung, *ChemPhysChem* **2016**, *17*, 433–442.
- [48] A. Hoffmann, M. T. Woodside, *Angew. Chem. Int. Ed.* **2011**, *50*, 12643–12646; *Angew. Chem.* **2011**, *123*, 12854–12857.
- [49] K. Bacia, Z. Petrásek, P. Schwill, *ChemPhysChem* **2012**, *13*, 1221–1231.
- [50] H. Yuan, M. Orrit, *ChemPhysChem* **2012**, *13*, 681–683.
- [51] J. P. Fouassier, F. Morlet-Savary, J. Lalevée, X. Allonas, C. Ley, *Materials* **2010**, *3*, 5130–5142.
- [52] T. Cordes, J. Vogelsang, P. Tinnefeld, *J. Am. Chem. Soc.* **2009**, *131*, 5018–5019.
- [53] K. Kitagawa, S. A. Blum, *ACS Catal.* **2017**, *7*, 3786–3791.
- [54] A. Biffis, P. Centomo, A. Del Zotto, M. Zecca, *Chem. Rev.* **2018**, *118*, 2249–2295.
- [55] P. Wang, J. Xia, Y. Gu, *Tetrahedron Lett.* **2015**, *56*, 6491–6494.
- [56] J. Yan, X. Wang, L. Zhou, L. Zhang, *RSC Adv.* **2017**, *7*, 20369–20372.
- [57] M. Navarro, S. Wang, H. Müller-Bunz, G. Redmond, P. Farràs, M. Albrecht, *Organometallics* **2017**, *36*, 1469–1478.
- [58] S. Sehayek, Y. Gidi, V. Glembocky, H. B. Brandaõ, P. François, G. Cosa, P. W. Wiseman, *ACS Nano* **2019**, *13*, 11955–11966.

Manuscript received: January 7, 2020
Revised manuscript received: February 15, 2020
Accepted manuscript online: February 18, 2020
Version of record online: April 1, 2020